Journal of the Mechanics and Physics of Solids 58 (2010) 1804–1818

Contents lists available at ScienceDirect

Journal of the Mechanics and Physics of Solids

journal homepage: www.elsevier.com/locate/jmps

Convex polynomial yield functions

Stefan Soare [a,*], Frédéric Barlat [b]

[a] Technical University of Cluj-Napoca, C. Daicoviciu 15, 400020 Cluj-Napoca, Romania
[b] Pohang University of Science and Technology, San 31 Hyoja-dong, Nam-gu, Pohang Gyeongbuk 790-784, Republic of Korea

ARTICLE INFO

Article history:
Received 5 April 2010
Received in revised form
11 August 2010
Accepted 15 August 2010

Keywords:
Anisotropy
Convex function
Polynomials
Sheet metal
Yield function

ABSTRACT

It is shown that some of the recently proposed orthotropic yield functions obtained through the linear transformation method are homogeneous polynomials. This simple observation has the potential to simplify considerably their implementation into finite element codes. It also leads to a general method for designing convex polynomial yield functions with powerful modeling capabilities. Convex parameterizations are given for the fourth, sixth and eighth order plane stress orthotropic homogeneous polynomials. Illustrations are shown for the modeling of biaxial and directional yielding properties of steel and aluminum alloy sheets. The parametrization method can be easily extended to general, 3D stress states.

1. Introduction

The concept of yield surface has been at the foundation of the theory of plasticity since its very beginnings (Tresca's 1864 experiments). The yield surface is, by definition, a surface in stress space bounding the set of all stress states for which a metallic material behaves elastically under external loading (time-independent conditions). Loading the material at stress states beyond this boundary causes irreversible, or plastic deformation of the material. While the concept of yield surface was initially an idea drawn upon observations at macroscopic, or continuum level, it soon found another fundamental application in the modeling of the plastic deformation of single crystals by the Schmid's (1931) law, and further of polycrystals by Taylor (1938) and Bishop and Hill (1951a,b). Polycrystal based calculations of the yield surface of BCC and FCC textured polycrystals brought an important insight regarding the yield surface: various combinations of textures and lattice classes feature significant differences in their *yield surface shapes*. In loose terms, steels (BCC class) exhibit in general smoother yield surfaces than aluminum alloys (FCC class), and both classes are bounded by the Tresca (inner bound) and von Mises (outer bound) surfaces. This led to generalizations of the von Mises function, by letting the homogeneity degree act as a parameter for describing yield surface shape, Hershey (1954) and Hosford (1972).

In this work we describe a broader generalization of the von Mises function based on Hershey and Hosford's idea. A phenomenological point of view is adopted and the flow potential is considered to be identical with the yield surface (associative plasticity). The quality of numerous predictions based on this simplified constitutive model (see below examples) can serve as a phenomenological, a posteriori argument to support this identification. A different kind of argument was supplied by Rice (1971). He concluded that this identification follows necessarily if "the local microstructural rearrangements proceed at rates governed by their associated thermodynamic forces". Thus, within this simplified framework, the yield surface determines the direction of plastic strain increment also (by the normality rule).

* Corresponding author.
E-mail addresses: stefan.soare@tcm.utcluj.ro, stef_soare@yahoo.com (S. Soare).

0022-5096/$ - see front matter © 2010 Elsevier Ltd. All rights reserved.
doi:10.1016/j.jmps.2010.08.005

This double role of the yield surface demands particular care for modeling both its values and gradient. Fortunately, such accuracy is not required to hold globally but only for local areas of the surface, those that are swept by the stress state during a specific loading program.

In general, only a limited number of experimental data points is available for yield function identification (simply because experiments are costly and difficult to conduct). In fact, for decades the standards of metal forming industry considered only the directional plastic properties as mechanical characteristics of sheet metals: the yield stress and r-value (the ratio of transverse to thickness strains) measured from uniaxial tensile tests performed on specimens cut out at several angles from the rolling direction. However, with computer simulations increasingly complementing experimental data, the demand for accurate constitutive modeling has also increased significantly. A necessary condition, then, is knowing what features of the yield surface require precise modeling so that sheet forming simulations will match accurately the outcome of characteristic experiments.

Two examples, of both practical and theoretical significance, will further illustrate the two basic features of an anisotropic yield function that were mentioned above: (1) it is now well established that the prediction of the limit strains of sheet metal under biaxial stretching depends considerably on the shape of the yield surface used to model the material, Bassani et al. (1979), Barlat (1987), Lian et al. (1989), and Soare (2010); (2) a good prediction of the earing profile of deep-drawn cups is possible within the framework of associative plasticity if the directional properties of the sheet are well described by the yield surface, Yoon et al. (2006) and Soare et al. (2008), and also if the pure shear (with respect to the symmetry axes of the sheet) yielding point is correctly represented, Soare and Banabic (2008). Therefore, as minimal requirements, a general purpose anisotropic yield function should be able to model accurately the directional properties of the sheet and to account for differences in yield surface shape between various classes of alloys.

Broadly speaking, there are three main approaches, or methods, for designing yield functions for anisotropic metals. One approach, historically the first, is to write polynomial expressions of the components of the stress tensor with respect to the symmetry axes of the material, with the added condition that these expressions be invariant with respect to the symmetry group of the material. In the case of an *orthotropic* sheet metal, the case of interest here, the most general polynomial form reads, for plane stress conditions, Hill (1950):

$$f^n(\sigma_x,\sigma_y,\sigma_{xy}) = \sum_{i+j+2k=n} A_{ijk}\sigma_x^i\sigma_y^j\sigma_{xy}^{2k} \tag{1}$$

where n is the homogeneity degree, and x, y and z denote the rolling, transverse and normal directions, respectively. Only yield functions which are symmetric about the origin of the stress space (tension/compression symmetry) will be considered and hence above the homogeneity degree is an even strictly positive integer.

The second method is based on representations of the symmetry group of the material in terms of a list of symmetry tensors/invariants, see for example Wang (1970), Liu (1982), and Boehler (1987). It generalizes the first method since any scalar function having as arguments the list of the invariants is a potential yield function.

While general in their approach, the above two methods do not deliver, in general, *convex* functions, and hence yield functions. Within the framework of associative plasticity, convexity is an essential property in two aspects (closely related): it allows for a consistent definition of the loading–unloading criterion, in the case of metals, and it guarantees a one-to-one relationship between the stress state and the rate of deformation. A third approach for designing anisotropic yield functions, with particular emphasis on convexity, has emerged during the early 1990s, Barlat et al. (1991), Karafillis and Boyce (1993), and evolved into a relatively well developed methodology for designing convex anisotropic functions, Barlat et al. (2005, 2007). This is the linear transformation method, which, in conjunction with the polynomial approach, makes the topic of this article: to find convex parameterizations for homogeneous polynomials and provide simple identification procedures for their parameters.

2. Isotropic generators, linear transformations and polynomials

In principle, the linear transformation method is quite straightforward. One starts with an *isotropic* function $\phi(\sigma_1,\sigma_2,\sigma_3)$, where σ_i are the principal values of the stress tensor σ, or its deviator. Then, to obtain an anisotropic function one substitutes the eigenvalues σ_i with those of an image stress tensor Σ defined by a linear transformation C as $\Sigma = C\sigma$. If S_i are the eigenvalues of Σ, then the anisotropic function is simply $f(\sigma) = \phi(S_1,S_2,S_3)$. In this context, the isotropic function ϕ plays the role of a *generator*. Two such generators have been favored from the beginning. One is the Hershey (1954)–Hosford (1972) function, HH for short:

$$2\phi^n(\sigma) = (\sigma_1-\sigma_2)^n + (\sigma_2-\sigma_3)^n + (\sigma_3-\sigma_1)^n \tag{2}$$

and the other is the Karafillis and Boyce (1993) function, KB for short:

$$[(2^n+2)/3^n]\phi^n(\sigma) = s_1^n + s_2^n + s_3^n \tag{3}$$

where s_i are the eigenvalues of the stress deviator $\sigma' \coloneqq \sigma - [\mathrm{tr}(\sigma)/3]I$. These two functions are symmetric (invariant to any permutation of their argument) and convex. A theorem of Davis (1957) states that if a function $f(M)$ defined on the space of $m \times m$ symmetric matrices can be represented as $f(M) = \phi(M_1,\ldots,M_m)$, with M_i the eigenvalues of M, then f is convex if ϕ is symmetric and convex. In our case: $f(\sigma) = \phi(T(\sigma))$, where $T(\sigma) = C\sigma$. Since composition with a linear function preserves

convexity, it follows that the anisotropic extension f is also convex. For an orthotropic, pressure independent material, the components of the (symmetric) image tensor with respect to the symmetry axes of the sheet are

$$\begin{aligned}
&\Sigma_x = \alpha_1\sigma_x + \alpha_2\sigma_y - (\alpha_1+\alpha_2)\sigma_z\\
&\Sigma_y = \alpha_3\sigma_x + \alpha_4\sigma_y - (\alpha_3+\alpha_4)\sigma_z\\
&\Sigma_z = \alpha_5\sigma_x + \alpha_6\sigma_y - (\alpha_5+\alpha_6)\sigma_z\\
&\Sigma_{xy} = \alpha_7\sigma_{xy}, \quad \Sigma_{xz} = \alpha_8\sigma_{xz}, \quad \Sigma_{yz} = \alpha_9\sigma_{yz}
\end{aligned} \tag{4}$$

with α_i the coefficients of the linear transformation, and the material parameters of the anisotropic yield function. With seven material parameters for plane stress states only mild variations in directional properties of the sheet can be modeled. In Barlat et al. (2005) the above theory was extended to incorporate several image tensors, thus improving its modeling capabilities. In what follows we analyze this extension and reveal its polynomial nature.

2.1. KB-based extension

Inspired by the works of Barlat et al. (2005) and Bron and Besson (2004), Plunkett et al. (2008) proposed the following extension of the KB function (3):

$$f^n(\sigma) = \sum_{k=1}^{K} f_k(\sigma) = \sum_{k=1}^{K} [(S_1^{(k)})^n + (S_2^{(k)})^n + (S_3^{(k)})^n] = \sum_{k=1}^{K} \mathrm{tr}[(\Sigma^{(k)})^n] \tag{5}$$

in which a number of K linear transformations $\Sigma^{(k)} = C^{(k)}\sigma$ is used, $S_i^{(k)}$ are the eigenvalues of the k-th image stress, and with obvious definitions for the f_k functions. Since each function $f_k^{1/n}$ is convex, a direct application of Minkowski's inequality will show that f is convex. Furthermore, each f_k is a homogeneous polynomial. Indeed, dropping for simplicity the subscript k, the eigenvalues S_i satisfy the characteristic equation

$$S_i^3 - I_1 S_i^2 - I_2 S_i - I_3 = 0 \tag{6}$$

with I_i the invariants of the image stress:

$$I_1 \coloneqq \mathrm{tr}(\Sigma), \quad I_2 \coloneqq (\Sigma\cdot\Sigma - I_1^2)/2, \quad I_3 \coloneqq \det(\Sigma) \tag{7}$$

By Eq. (4), I_i, i=1,2,3, are homogeneous polynomials of first, second and third order, respectively, in the parameters α_j and stress components σ_{pq}. Next, we record the trivial relations:

$$Q_1 \coloneqq S_1 + S_2 + S_3 = I_1, \quad Q_2 \coloneqq S_1^2 + S_2^2 + S_3^2 = \Sigma\cdot\Sigma = I_1^2 + 2I_2 \tag{8}$$

Multiplying Eq. (6) with S_i^{p-3} and then adding the three resulting relations leads to the following recurrence formula for the sums of powers $Q_p \coloneqq S_1^p + S_2^p + S_3^p, p \geq 3$:

$$Q_p = I_1 Q_{p-1} + I_2 Q_{p-2} + I_3 Q_{p-3} \tag{9}$$

From Eqs. (8) and (9) it follows, by induction, that Q_p is a p-th order homogeneous polynomial of the components of the stress tensor.

2.2. HH-based extension

In Barlat et al. (2005) the HH function (2) was extended to an anisotropic function by the use of two linear transformations as follows:

$$\begin{aligned}
f^n(\sigma) = \phi(S_1^{(1)}, S_2^{(1)}, S_3^{(1)}, S_1^{(2)}, S_2^{(2)}, S_3^{(2)}) &= (S_1^{(1)} - S_1^{(2)})^n + (S_1^{(1)} - S_2^{(2)})^n + (S_1^{(1)} - S_3^{(2)})^n + (S_2^{(1)} - S_1^{(2)})^n + (S_2^{(1)} - S_2^{(2)})^n + (S_2^{(1)} - S_3^{(2)})^n\\
&+ (S_3^{(1)} - S_1^{(2)})^n + (S_3^{(1)} - S_2^{(2)})^n + (S_3^{(1)} - S_3^{(2)})^n
\end{aligned} \tag{10}$$

with $S_i^{(k)}$, for k=1,2, the eigenvalues of the image tensors $\Sigma^{(k)} = C^{(k)}\sigma$. Similarly with the Plunkett extension of the KB function, one could, at least in principle, arbitrarily increase the modeling capabilities by considering an arbitrary number of image tensors and write, for example, the following extension:

$$f^n(\sigma) = \phi(S_1^{(1)}, S_2^{(1)}, S_3^{(1)}, \ldots, S_1^{(K)}, S_2^{(K)}, S_3^{(K)}) = \sum_{p<q}^{K} \phi_{pq}(S_1^{(p)}, S_2^{(p)}, S_3^{(p)}, S_1^{(q)}, S_2^{(q)}, S_3^{(q)}) \tag{11}$$

Davis' theorem stated in the introduction to this section admits the following generalization applicable when several image stresses are used as arguments: let $f(M^{(1)},\ldots,M^{(K)})$ be a real function defined on the direct product of K copies of the space of symmetric $n\times n$ real matrices. Suppose the function f admits the spectral representation

$$f(M^{(1)},\ldots,M^{(K)}) = \phi(M_1^{(1)},\ldots,M_n^{(1)},\ldots,M_1^{(K)},\ldots,M_n^{(K)}) \tag{12}$$

where $M_i^{(k)}$ are the eigenvalues of $M^{(k)}$. Then f is convex if the function ϕ has the following symmetry property:

$$\phi(M_1^{(1)},\ldots,M_n^{(1)},\ldots,M_1^{(K)},\ldots,M_n^{(K)}) = \phi(M_{\tau_1(1)}^{(1)},\ldots,M_{\tau_1(n)}^{(1)},\ldots,M_{\tau_K(1)}^{(K)},\ldots,M_{\tau_K(n)}^{(K)}) \tag{13}$$

for any K permutations τ_k of the set $\{1,\ldots,n\}$, and if ϕ is convex.

The anisotropic extension (10) is a homogeneous polynomial. Indeed, with Newton's binomial formula we have

$$(S_i^{(1)}-S_1^{(2)})^n+(S_i^{(1)}-S_2^{(2)})^n+(S_i^{(1)}-S_3^{(2)})^n = \sum_{p=0}^{n}(-1)^p C_n^p (S_i^{(1)})^{n-p}[(S_1^{(2)})^p+(S_2^{(2)})^p+(S_3^{(2)})^p] \tag{14}$$

where $C_n^p = n!/[p!(n-p)!]$. Adding the above identities for $i=1,2,3$ gets us

$$f^n(\sigma) = \sum_{p=0}^{n}(-1)^p C_n^p Q_{n-p}(\Sigma^{(1)})Q_p(\Sigma^{(2)}) \tag{15}$$

The conclusion follows from the results in the previous subsection.

2.3. Further discussion

We have shown that the linear transformation approach with the HH and KB inspired generators leads to polynomial formulations. In fact, each particular formulation studied here can be viewed as a *method* for identifying the coefficients of a polynomial (of appropriate degree) so that to obtain a convex polynomial. This is important: while polynomial expressions are simple to generate and manipulate (and hence their attractiveness for computer implementations), obtaining by default convex polynomials is a difficult (NP-hard) problem. The number of linear transformations that can be used without introducing redundant parameters is limited. This follows from the fact that the space of homogeneous polynomials of a certain degree is finite dimensional. The subset of polynomial (convex) yield functions is a *convex cone* of this space. To show this, let P_n and Q_n denote two homogeneous polynomials of degree n, with $P_n \geq 0$, $Q_n \geq 0$, $P_n^{1/n}$ and $Q_n^{1/n}$ convex. With $R_n = (1-\lambda)P_n + \lambda Q_n$, for some $\lambda \in [0,1]$, the following inequalities hold for $\sigma = (1-a)\sigma_1 + a\sigma_2$, with $a \in [0,1]$ and $\sigma_1,\sigma_2 \in \mathbb{R}^6$:

$$\begin{aligned} R_n^{1/n}(\sigma) &= \{[(1-\lambda)^{1/n}P_n^{1/n}(\sigma)]^n + [\lambda^{1/n}Q_n^{1/n}(\sigma)]^n\}^{1/n} \\ &\leq \{[(1-\lambda)^{1/n}((1-a)P_n^{1/n}(\sigma_1)+aP_n^{1/n}(\sigma_2))]^n + [\lambda^{1/n}((1-a)Q_n^{1/n}(\sigma_1)+aQ_n^{1/n}(\sigma_2))]^n\}^{1/n} \\ &\leq (1-a)R_n^{1/n}(\sigma_1)+aR_n^{1/n}(\sigma_2) \end{aligned} \tag{16}$$

the second inequality above being a consequence of Minkowski's inequality. Equivalently, if (A_i) denotes the vector of coefficients of the homogeneous polynomial P_n, then the set

$$C_n := \{(A_i) \in \mathbb{R}^N | P_n \geq 0 \text{ and } P_n^{1/n} \text{ is convex}\} \tag{17}$$

is a convex cone in $\mathbb{R}^N$, where N is the dimension of the space of homogeneous polynomials of degree n.

In what follows we generalize the linear transformation approach and develop convex parameterizations for the fourth, sixth and eighth order *plane stress* polynomials. Extensions to full 3D stress states are discussed in the concluding section. We begin by describing an important subset of C_n: the cone of in-plane isotropic polynomials.

3. In-plane isotropic plane stress polynomial generators

The HH and KB functions (2) and (3) are homogeneous polynomials. Here it is shown that within the polynomial family they admit much more flexible generalizations. First, the general theory is synthesized in three Lemmas. The plane stress state is assumed parallel with the plane (x,y) of the sheet.

Lemma 1. *Every in-plane isotropic plane stress function is uniquely determined by its restriction to the biaxial plane (x,y), that is, by its biaxial curve.*

Proof. Let $f(\sigma_x,\sigma_y,\sigma_{xy})$ denote a plane stress function, and $g(\sigma_x,\sigma_y) := f(\sigma_x,\sigma_y,0)$ denote its biaxial restriction. Since f is invariant with respect to rotations about the z-axis, and since for every stress state $(\sigma_x,\sigma_y,\sigma_{xy})$ there exits a rotation about the z-axis that reduces its components to $(\sigma_1,\sigma_2,0)$, we have: $f(\sigma_x,\sigma_y,\sigma_{xy}) = f(\sigma_1,\sigma_2,0) = g(\sigma_1,\sigma_2)$. □

The next two results give conditions that in-plane isotropic plane stress functions be convex.

Lemma 2. *An in-plane isotropic plane stress function f is convex if and only if its biaxial curve is convex.*

Proof. According to Lemma 1, we have $f(\sigma_x,\sigma_y,\sigma_{xy}) = g(\sigma_1,\sigma_2)$, with σ_i the principal stresses of σ. Since f is in-plane isotropic, g must be symmetric. Then, if g is convex, with Davis's theorem it follows that f is convex. □

Lemma 3 (*Flanders, 1968*). *Let $g : \mathbb{R}^2 \longrightarrow \mathbb{R}_+$ be positive first order homogeneous, and $h(\omega) := g(\cos\omega,\sin\omega), \omega \in [0,2\pi)$, denote its restriction to the unit circle. Then g is convex if and only if*

$$h''(\omega)+h(\omega) \geq 0, \quad \omega \in [0,\pi) \tag{18}$$

Proof. Writing the Hessian H of g in the polar coordinates (r,ω) associated to a Cartesian coordinate system xy, by employing the first order homogeneity of g, i.e., $g(r,\omega)=rh(\omega)$, we obtain

$$H[v,v] \coloneqq (H:v)\cdot v = \frac{h''(\omega)+h(\omega)}{r}(v_1\cos\omega - v_2\sin\omega)^2$$

for any vector $v=[v_1,v_2]^T$. We have $H[v,v]\geq 0$ if and only if Eq. (18) holds. □

In the present case the yield function has the form

$$f(\sigma_x,\sigma_y,\sigma_{xy}) = g(\sigma_1,\sigma_2) = [P_n(\sigma_1,\sigma_2)]^{1/n} \tag{19}$$

with P_n a homogeneous polynomial of degree n. Then Eq. (18) becomes

$$n^2 g_n^2 - (n-1)(g_n')^2 + n g_n g_n'' \geq 0, \quad \omega\in[-\pi/4,\pi/4] \tag{20}$$

where $g_n(\omega) \coloneqq P_n(\cos\omega,\sin\omega)$, the range of ω being restricted by symmetry considerations (in-plane isotropy).

3.1. n=4 (fourth order in-plane isotropic)

The most general in-plane isotropic fourth order polynomial is as follows:

$$IP_4(\sigma) = a_1(\sigma_1^4+\sigma_2^4) + a_2(\sigma_1^3\sigma_2+\sigma_1\sigma_2^3) + a_3\sigma_1^2\sigma_2^2 \tag{21}$$

The coefficients a_i are determined so that the above biaxial curve fits the yield stress $\overline{\sigma}$, the average r-value R, and the balanced biaxial yield stress $(\overline{\sigma}_b,\overline{\sigma}_b)$ (an overline denoting normalization with some constant):

$$a_1 = \frac{1}{\overline{\sigma}_0^4}, \quad a_2 = \frac{-4a_1R}{1+R}, \quad a_3 = \frac{1}{\overline{\sigma}_b^4} - 2(a_1+a_2) \tag{22}$$

Assuming a_1 and a_2 identified, the input data point $\overline{\sigma}_b$ can only take values consistent with the convexity restriction upon the biaxial curve. Eq. (20) becomes in this case

$$G(\omega,a_3) \coloneqq C_0 a_3^2 + C_1 a_3 + C_2 \geq 0 \tag{23}$$

where

$$C_0 \coloneqq [\cos(4\omega)-1]/2, \quad C_1 \coloneqq 2[3a_1 + a_1\cos(4\omega) - a_2\sin(2\omega)]$$

$$C_2 \coloneqq 3[4a_1a_2\sin(2\omega) - a_2^2(1+\cos(4\omega))/2 + 2a_1^2(1-\cos(4\omega))] \tag{24}$$

Inequality (23) can be solved numerically for the maximum convexity interval $A_3\leq a_3\leq B_3$ as follows. First, one takes a fine grid $\{\omega_i\}_i$ over the interval $[-\pi/4,\pi/4]$. Then, by trial and error one finds one solution of (23), say a_3', with $G(\omega_i,a_3')\geq 0$ for all i (for example, in the isotropic case an a priori solution is Mises[2]). After finding one solution, with a trial and error procedure one searches for the biggest $\delta>0$ such that $A_3 \coloneqq a_3'-\delta$ satisfies $G(\omega_i,A_3)\geq 0$ for all i. The upper bound $B_3 \coloneqq a_3'+\delta$ is found similarly. An alternative is to solve directly the quadratic (for $\omega\neq 0$ or $\pi/4$) equation $G(\omega,a_3)=0$, with G given by (23), for the two solutions $x_1(\omega)\leq x_2(\omega)$ and then $A_3=\max\{x_1(\omega)|\omega\in[-\pi/4,\pi/4]\}$, $B_3=\min\{x_2(\omega)|\omega\in[-\pi/4,\pi/4]\}$. This method will be used and illustrated in what follows.

3.2. n=6 (sixth order in-plane isotropic)

The most general in-plane isotropic sixth order polynomial reads

$$IP_6(\sigma) = a_1(\sigma_1^6+\sigma_2^6) + a_2(\sigma_1^5\sigma_2+\sigma_1\sigma_2^5) + a_3(\sigma_1^4\sigma_2^2+\sigma_1^2\sigma_2^4) + a_4\sigma_1^3\sigma_2^3 \tag{25}$$

The coefficients a_i can be determined so that the above biaxial curve fits the yield stress $\overline{\sigma}_0$ along the x-axis, the average r-value R, or the r-value along the x-axis, r_0, the balanced biaxial yield stress $(\overline{\sigma}_b,\overline{\sigma}_b)$, and one additional point on the biaxial curve. This second point is defined as follows. On the segment joining the points $(\overline{\sigma}_0,0)$ and $(\overline{\sigma}_b,\overline{\sigma}_b)$ let $M=[(\overline{\sigma}_0,0)+(\overline{\sigma}_b,\overline{\sigma}_b)]/2$ denote its middle point. Then the line joining the origin (0,0) and M will intersect the biaxial curve at the point of coordinates $(\overline{\sigma}_x,t\overline{\sigma}_x)$ with the ratio t defined by

$$t \coloneqq \overline{\sigma}_b/(\overline{\sigma}_b+\overline{\sigma}_0) \tag{26}$$

We define the *shape parameter*

$$P \coloneqq \overline{\sigma}_0/\overline{\sigma}_x \tag{27}$$

In what follows we choose as normalizing constant the yield stress along the rolling direction σ_0 (so that $\overline{\sigma}_0=1$; any other yield stress can be chosen as normalizing constant but then either the previous or the following equation should be modified accordingly). The additional equation stating that the point $(\overline{\sigma}_x,t\overline{\sigma}_x)$ is on the biaxial curve is then

$$P^6 = a_1(1+t^6) + a_2(t+t^5) + a_3(t^2+t^4) + a_4t^3 \tag{28}$$

The parameters a_i in Eq. (25) are then determined by the following formulas:

$$a_1 = \frac{1}{\overline{\sigma}_0} = 1, \quad a_2 := \frac{-6a_1R}{1+R}, \quad a_3 = \frac{D_1}{D_2}, \quad a_4 = \frac{D_3 - D_4}{D_2} \tag{29}$$

$$D_1 := P^6 - a_1(1+t^6) - a_2 t(1+t^4) - t^3[1/\overline{\sigma}_b^6 - 2(a_1+a_2)], \quad D_2 := t^2(1-t)^2 \tag{30}$$

$$D_3 := t^2(1+t^2)[1/\overline{\sigma}_b^6 - 2(a_1+a_2)], \quad D_4 := 2[P^6 - a_1(1+t^6) - a_2 t(1+t^4)] \tag{31}$$

Convexity of the biaxial curve restricts the variation of the parameter P to a certain convexity interval $[P_1,P_2]$. This interval can be determined by either one of the procedures described for IP_4, where this time the quadratic that must be positive is

$$G(\omega,P^6) := \sum_{1 \le i \le j \le 4} c_{ij}(\omega) a_i a_j \ge 0, \quad \omega \in [-\pi/4, \pi/4] \tag{32}$$

with the coefficients c_{ij} listed in Appendix A. In what follows we use the second approach an reduce the above inequality to a quadratic inequality for the shape parameter P (actually for P^6) by making the substitutions (29). Using the appropriate formulas in Appendix A, the coefficient of the quadratic term in P^6 is found to be

$$\frac{1}{D_2}(c_{33} - 2c_{34} + 4c_{44}) = \frac{-1}{D_2}[1 - \cos^2(2\omega)][2 - \sin(2\omega)][1 - \sin(2\omega)] \le 0 \tag{33}$$

Hence the convexity set is indeed an interval given by similar max/min formulas as for IP_4 (as expected, since the convexity set is convex, by Section 2.3).

As illustration of IP_6 we consider the important case of an isotropic material: $\overline{\sigma}_0 = \overline{\sigma}_b = R = 1$. The two solutions $P_1^6(\omega) = x_1(\omega) < x_2(\omega) = P_2^6(\omega)$, $\omega \in [-\pi/4, \pi/4]$, of the equation $G(\omega,P^6) = 0$ are plotted in Fig. 1. By taking a fine grid over $[-\pi/4, \pi/4]$ one identifies the convexity interval as

$$\max\{P_1(\omega) | \omega \in [-\pi/4, \pi/4]\} = 0.810 \le P \le 0.926 = \min\{P_2(\omega) | \omega \in [-\pi/4, \pi/4]\} \tag{34}$$

When the coefficients of IP_6 are already known, one can compute the corresponding shape parameter of the point on the biaxial curve with the stress ratio $t = 1/2$ (when $\overline{\sigma}_0 = \overline{\sigma}_b$). For the Mises function this point corresponds to the plane strain point:

$$P^6 = (1 - 1/2 + (1/2)^2)^3 \Longrightarrow P = \sqrt{3}/2 \approx 0.866 \tag{35}$$

Similarly one finds that the HH biaxial curve has the shape parameter $P = (33/64)^{1/6} \approx 0.895$, and the KB function $P = (243/704)^{1/6} \approx 0.837$, both for $n = 6$. Conversely, if the coefficients a_i of IP_6 are computed with $\overline{\sigma}_0 = \overline{\sigma}_b = R = 1$ and: $P = \sqrt{3}/2$, then one obtains the von Mises function; $P = (33/64)^{1/6}$, then one obtains the HH function, and $P = (243/704)^{1/6}$ then one obtains the KB function (their plane stress restrictions). These curves, together with the two extreme curves (corresponding to the two extreme values of the shape parameters), are shown in Fig. 2.

3.3. n=8 (eighth order in-plane isotropic)

The most general in-plane isotropic eighth order polynomial reads

$$IP_8(\sigma) = a_1(\sigma_1^8 + \sigma_2^8) + a_2(\sigma_1^7\sigma_2 + \sigma_1\sigma_2^7) + a_3(\sigma_1^6\sigma_2^2 + \sigma_1^2\sigma_2^6) + a_4(\sigma_1^5\sigma_2^3 + \sigma_1^3\sigma_2^5) + a_5\sigma_1^4\sigma_2^4 \tag{36}$$

The coefficients a_i can be determined so that the above biaxial curve fits the yield stress $\overline{\sigma}_0$ along the x-axis, the average r-value R, or the r-value along the x-axis, r_0, the balanced biaxial yield stress $(\overline{\sigma}_b, \overline{\sigma}_b)$, and two additional points on the biaxial curve. One of them is the plane strain neighbor $(\overline{\sigma}_x, t\overline{\sigma}_x)$, with $t := \overline{\sigma}_b/(\overline{\sigma}_b + \overline{\sigma}_0)$, as defined previously for IP_6, with the associated shape parameter $P_1 := \sigma_0/\sigma_x$. We choose the other point on the bisectrix of the fourth (or second) quadrant

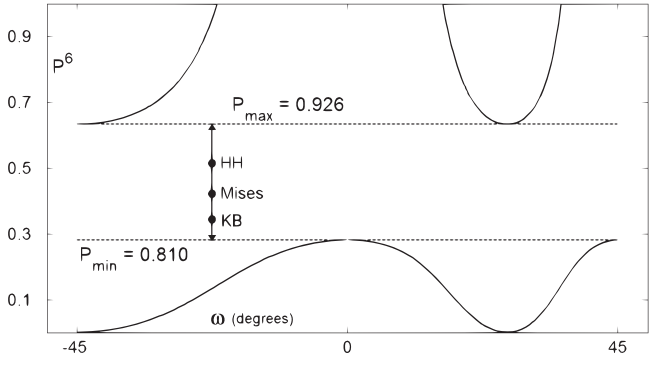

Fig. 1. Convexity interval for IP_6 in the isotropic case: the lower and upper bounds of the shape parameter deduced from the quadratic G in Eq. (32).

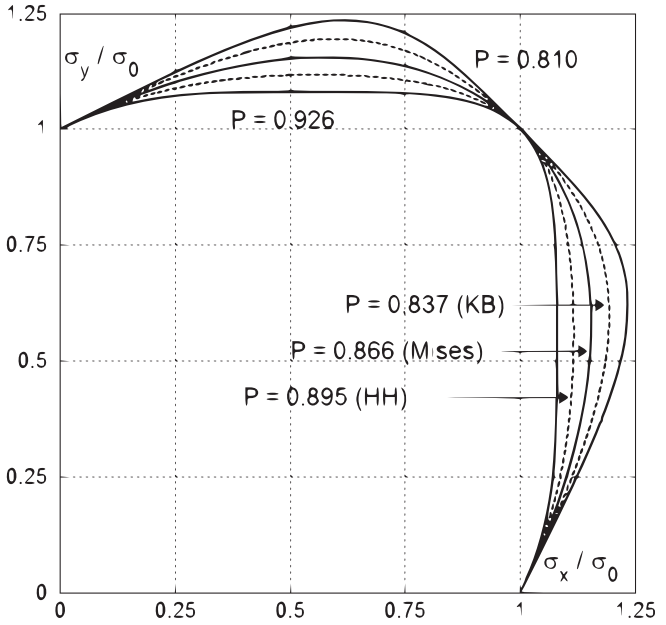

Fig. 2. Several IP_6 isotropic biaxial curves: Mises, HH, KB, and the two extreme bounds.

(the pure shear yielding point), $(\overline{\sigma}_y,-\overline{\sigma}_y)$, with the second shape parameter:

$$P_2 \coloneqq \overline{\sigma}_0/\overline{\sigma}_y \tag{37}$$

The conditions that these two additional points be on the biaxial curve are

$$P_1^8 = a_1(1+t^8)+a_2(t+t^7)+a_3(t^2+t^6)+a_4(t^3+t^5)+a_5t^4$$

$$P_2^8 = 2a_1-2a_2+2a_3-2a_4+a_5 \tag{38}$$

Solving the five resulting equations for the coefficients a_i one obtains the following solution with two parameters P_i:

$$a_1 = \frac{1}{\overline{\sigma}_0^8} = 1, \quad a_2 = \frac{-8a_1R}{1+R}, \quad a_4 = \frac{1}{4}\left(\frac{1}{\overline{\sigma}_b^8}-P_2^8-4a_2\right), \quad a_3 = A-\frac{t^4}{2}B, \quad a_5 = \frac{t^2+t^6}{2}B-2A$$

$$A \coloneqq \frac{P_1^8-a_1(1+t^8)-a_2t(1+t^6)-a_4t^3(1+t^2)}{t^2(1-t^2)^2}, \quad B \coloneqq \frac{(1/\overline{\sigma}_b^8)+P_2^8-4a_1}{t^2(1-t^2)^2} \tag{39}$$

The two parameters P_1^8 and P_2^8 are subject to the quadratic convexity constraint (20) which in this case becomes

$$G(\omega,P_1^8,P_2^8) \coloneqq \sum_{1\le i\le j\le 5} c_{ij}(\omega)a_ia_j \ge 0, \quad \omega\in[-\pi/4,\pi/4] \tag{40}$$

with the c_{ij} coefficients listed in Appendix A. The convexity set is thus

$$IC_8 \coloneqq \bigcap_{-\pi/4\le\omega\le\pi/4} \{(P_1^8,P_2^8)\in\mathbb{R}^2 | G(\omega,P_1^8,P_2^8)\ge 0\} \tag{41}$$

For practical purposes, this set can be described by the trial and error procedure described for IP_4 and IP_6: starting from a point $(Q_1,Q_2)\in IC_8$, one finds the maximal interval $[Q_2-\delta_1,Q_2+\delta_2]$ such that the segment $\{Q_1\}\times[Q_2-\delta_1,Q_2+\delta_2]\subset IC_8$; then one increments/decrements Q_1 and finds the new corresponding segment and so on. A complementary graphical procedure, that can give a useful global picture of IC_8, is to plot for values ω_i at points of a grid on $[-\pi/4,\pi/4]$ the quadratics (and also lines, for some values of ω) $G(\omega_i,Q_1,Q_2)=0$ for $(Q_1,Q_2)\in(0,1)\times[1,256]$. Then the boundary of the convexity set will appear as an envelope of the set of constraints (though only portions of this boundary are envelopes in the strict sense of the definition).

As for IP_6, we illustrate IP_8 in the completely isotropic case: $\overline{\sigma}_0=\overline{\sigma}_b=R=1$. The von Mises function (Mises^4) is characterized by $P_1=\sqrt{3}/2$ and $P_2=\sqrt{3}\approx 1.732$; the HH function is characterized by $P_1=(129/256)^{1/8}\approx 0.918$ and $P_2=129^{1/8}\approx 1.836$; the KB function is characterized by $P_1=(2187/11\,008)^{1/8}\approx 0.817$ and $P_2=(2187/43)^{1/8}\approx 1.634$. The entire set of admissible shape parameters P_1 and P_2 in this case is shown in Fig. 3. Remarkably, this set has four vertices (and almost straight edges). They can be calculated by the trial and error procedure mentioned above. Starting from the

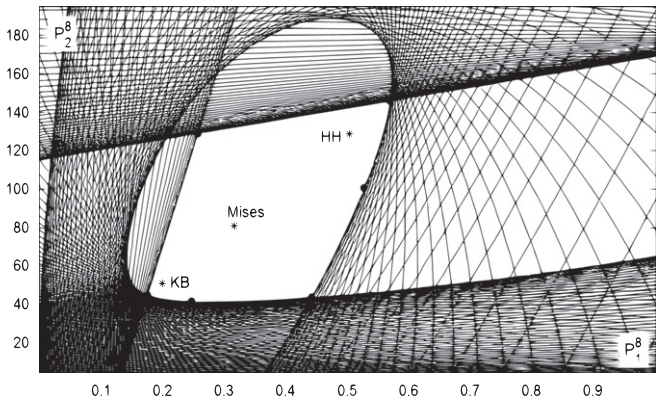

Fig. 3. The convexity set IC_8 for IP_8 in the isotropic case. Important inner points marked with stars: KB, Mises and HH. Generating vertices on the boundary marked with full circles.

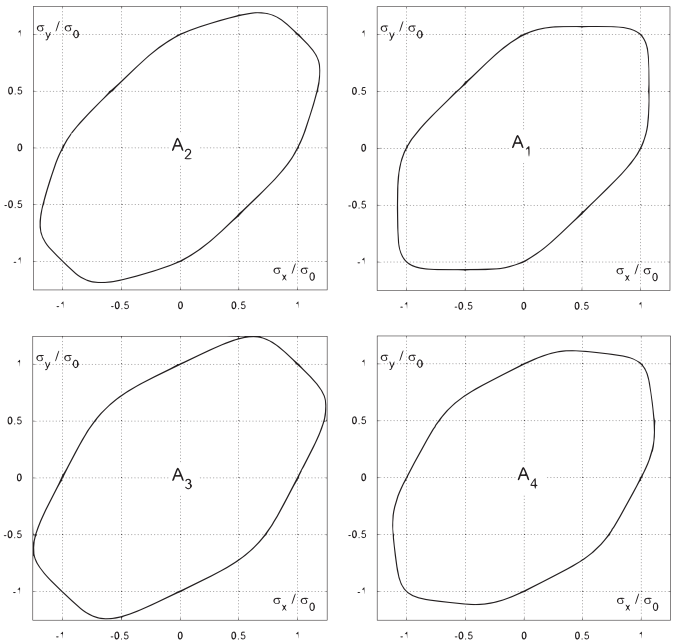

Fig. 4. The IP_8 biaxial curves corresponding to the four vertices of the IC_8 set, Eq. (42).

upper right vertex and moving counterclockwise these vertices are

$$A_1 = (0.569,145.7), \quad A_2 = (0.2577,128.8), \quad A_3 = (0.1758,45), \quad A_4 = (0.4417,43.9) \tag{42}$$

corresponding to the shape parameters (0.932,1.864), (0.8441,1.8355), (0.8047,1.6095), and (0.9029,1.6045), respectively. Given the shape of IC_8 in this case, that is, close to a quadrilateral, the convex hull of the four vertices (42) can serve as a good approximation (from within) of the convexity set IC_8 itself. Thus the pairs of shape parameters

$$(P_1^8, P_2^8) = \lambda_1 A_1 + \lambda_2 A_2 + \lambda_3 A_3 + \lambda_4 A_4, \quad \sum_{i=1}^{4} \lambda_i = 1, \ 0 \le \lambda_i \tag{43}$$

are always associated with a convex biaxial curve. If needed, one can further refine this approximation by adding more boundary points. For example, by adding just two more vertices, A_5=(0.2478, 41.67) and A_6 = (0.5267, 100.77), corresponding to the shape parameters (0.840, 1.594) and (0.923, 1.78), respectively, one obtains a fairly complete description of IC_8.

The biaxial curves corresponding to the four vertices in Eq. (42) are shown in Fig. 4. The curve in the isotropic IP_8 family that is closest to the Tresca's hexagon is characterized by vertex A_1. In particular, the A_1-curve is interior to the HH biaxial curve. At the opposite extreme is the biaxial curve characterized by vertex A_3. Every other point of IC_8 will generate a

biaxial curve that lies between these two extremes. For comparison, the tightest shape in the isotropic IP_6 family is obtained for P=0.926. The second shape parameter for IP_6 is then uniquely determined by $P_2^6 = 2(a_1-a_2+a_3)-a_4$=1.852. Hence the tightest IP_6 biaxial curve lies between the A_1 and HH curves of the IP_8 family.

4. Convex orthotropic plane stress polynomials

For a plane stress analysis the image stress takes the form

$$\Sigma = \begin{bmatrix} \beta_1\sigma_x+\beta_2\sigma_y & \beta_5\sigma_{xy} \\ \beta_5\sigma_{xy} & \beta_3\sigma_x+\beta_4\sigma_y \end{bmatrix} \tag{44}$$

The above formula is a restriction of Eq. (4), having only five parameters per image stress. Other parameterizations based on yield functions with a 3D stress state as argument may take advantage of the full set of seven parameters characterizing their plane stress restrictions. One example is the Yld2004 function, Barlat et al. (2005).

We propose the following parametrization for an orthotropic polynomial P_n:

$$P_n(\sigma_x,\sigma_y,\sigma_{xy}) = \frac{1}{K}\sum_{k=1}^{K} IP_n^{(k)}(S_1^{(k)},S_2^{(k)}) \tag{45}$$

with K the number of image stresses, with $IP_n^{(k)}$ the in-plane isotropic generator corresponding to the image stress $\Sigma^{(k)}$, and $S_i^{(k)}$ the eigenvalues of $\Sigma^{(k)}$. These eigenvalues are solutions of the characteristic equation:

$$S_i^2 - I_1 S_i + I_2 = 0 \tag{46}$$

with $I_1 := \mathrm{tr}(\Sigma), I_2 := \det(\Sigma)$. Then for $Q_p(\Sigma) := S_1^p + S_2^p$ the following recurrence formula holds:

$$Q_p = I_1 Q_{p-1} - I_2 Q_{p-2}, \quad p \geq 2 \tag{47}$$

Furthermore, for $i > j \geq 0$ and with $i+j=n$ we have

$$S_1^i S_2^j + S_1^j S_2^i = I_2^j Q_{i-j} \tag{48}$$

Hence the right-hand member of Eq. (45) is indeed an n-th order homogeneous polynomial. Formulas (44) and (45), (47) and (48), together with the corresponding generator, (21), or (25), or (36), can be used to find the explicit form of the parametrization of the coefficients of the following polynomials:

$$P_4 = A_1\sigma_x^4 + A_2\sigma_x^3\sigma_y + A_3\sigma_x^2\sigma_y^2 + A_4\sigma_x\sigma_y^3 + A_5\sigma_y^4 + (A_6\sigma_x^2 + A_7\sigma_x\sigma_y + A_8\sigma_y^2)\sigma_{xy}^2 + A_9\sigma_{xy}^4 \tag{49}$$

$$\begin{aligned} P_6 = {} & A_1\sigma_x^6 + A_2\sigma_x^5\sigma_y + A_3\sigma_x^4\sigma_y^2 + A_4\sigma_x^3\sigma_y^3 + \cdots + A_7\sigma_y^6 + (A_8\sigma_x^4 + A_9\sigma_x^3\sigma_y + A_{10}\sigma_x^2\sigma_y^2 + A_{11}\sigma_x\sigma_y^3 + A_{12}\sigma_y^4)\sigma_{xy}^2 \\ & + (A_{13}\sigma_x^2 + A_{14}\sigma_x\sigma_y + A_{15}\sigma_y^2)\sigma_{xy}^4 + A_{16}\sigma_{xy}^6 \end{aligned} \tag{50}$$

$$\begin{aligned} P_8 = {} & A_1\sigma_x^8 + A_2\sigma_x^7\sigma_y + A_3\sigma_x^6\sigma_y^2 + A_4\sigma_x^5\sigma_y^3 + A_5\sigma_x^4\sigma_y^4 + \cdots + A_9\sigma_y^8 + (A_{10}\sigma_x^6 + A_{11}\sigma_x^5\sigma_y + A_{12}\sigma_x^4\sigma_y^2 + A_{13}\sigma_x^3\sigma_y^3 + \cdots + A_{16}\sigma_y^6)\sigma_{xy}^2 \\ & + (A_{17}\sigma_x^4 + A_{18}\sigma_x^3\sigma_y + A_{19}\sigma_x^2\sigma_y^2 + A_{20}\sigma_x\sigma_y^3 + A_{21}\sigma_y^4)\sigma_{xy}^4 + (A_{22}\sigma_x^2 + A_{23}\sigma_x\sigma_y + A_{24}\sigma_y^2)\sigma_{xy}^6 + A_{25}\sigma_{xy}^8 \end{aligned} \tag{51}$$

Eqs. (49)–(51) are the formulations to be used, for example, in an FE simulation. The formulas for computing the coefficients $A_i = A_i(a_p,\beta_q)$, after identifying the set of parameters (a_p,β_q), are listed for n=4,6,8, in the electronic version of the paper (as supplementary material). An alternative implementation of P_n using Eq. (45) can follow the model in Appendix B. The advantage of this alternative is that the implementation can easily vary the degree n. For large exponents n it also requires less arithmetic operations. On the other hand, for plane stress applications with input data from mechanical tests, n=6 already provides significant modeling capabilities, while n=8 seems more than sufficient. Finally, in the present parametrization each polynomially generated function (i.e., $P_n^{1/n}$) is convex since each $IP_n^{1/n}$ is convex and then $P_n^{1/n}$ is convex (by a simple application of Minkowski's inequality).

The parameters a_p and β_q, and hence A_i, are determined so that they optimize the distance between predicted and experimental biaxial and directional data. In what follows by Y_θ, R_θ and Y_b, R_b are denoted the experimentally measured yield stress and r-value for a uniaxial traction test in a direction making an angle θ with the rolling axis, and the measured balanced-biaxial yield stress and r-value, respectively. With σ_θ and r_θ we shall denote the P_n predicted yield stress and r-values for the same experiment, while σ_b and r_b denote the predictions for the balanced-biaxial stress state. An overline indicates normalization with the yield stress along the rolling direction ($\overline{Y}_\theta = Y_\theta/Y_0$, etc.). P_n predicted directional and balanced-biaxial properties are

$$(\overline{\sigma}_\theta)^{-n} = P_n(\cos^2\theta,\sin^2\theta,\sin\theta\cos\theta) =: S_\theta(A_i) \tag{52}$$

$$r_\theta = \left(\frac{\partial P_n}{\partial\sigma_{xy}}\sin\theta\cos\theta - \frac{\partial P_n}{\partial\sigma_x}\sin^2\theta - \frac{\partial P_n}{\partial\sigma_y}\cos^2\theta\right) \Big/ \left(\frac{\partial P_n}{\partial\sigma_x} + \frac{\partial P_n}{\partial\sigma_y}\right) =: \frac{B_\theta(A_i)}{C_\theta(A_i)} \tag{53}$$

where above the partial derivatives are computed at the point $(\cos^2\theta, \sin^2\theta, \sin\theta\cos\theta)$, and

$$(\overline{\sigma}_b)^{-n} = P_n(1,1,0) =: S_b(A_i), \quad r_b = \frac{\partial P_n}{\partial \sigma_y}(1,1,0) \Big/ \frac{\partial P_n}{\partial \sigma_x}(1,1,0) = \frac{B_b(A_i)}{C_b(A_i)} \tag{54}$$

The distance function to be minimized with respect to the material parameters is then

$$g(a_p^{(k)}, \beta_i^{(k)}) = \frac{1}{2}\sum_{j=1}^{J}\left\{ w_j^s[S_{\theta_j} - (\overline{Y}_{\theta_j})^{-6}]^2 + w_j^r\left[\frac{B_{\theta_j}}{C_{\theta_j}} - R_{\theta_j}\right]^2\right\} + \frac{1}{2}\left\{ w_b^s[S_b - (\overline{Y}_b)^{-6}]^2 + w_b^r\left[\frac{B_b}{C_b} - R_b\right]^2\right\} \tag{55}$$

where J is the number of directional data points (usually $3 \le J \le 7$), and the w's are weights for adjusting the fit of each data point. For implementation purposes it helps noting that the S, B and C functions in Eqs. (52)–(54) can be calculated with simple dot product formulas. For example

$$S = V \cdot X \quad \text{with} \begin{cases} X := [s_x^n, s_x^{n-1}s_y, \ldots, s_y^n, s_x^{n-2}s_{xy}^2, \ldots, s_{xy}^n] \\ V := [A_1, A_2, \ldots, A_{n+1}, A_{n+2}, \ldots] \end{cases} \tag{56}$$

the coefficients vector V being the sum of the vectors of coefficients of P_n corresponding to each image stress:

$$V = \frac{1}{K}\sum_{k=1}^{K} V^{(k)}(\beta_1^{(k)}, \beta_2^{(k)}, \beta_3^{(k)}, \beta_4^{(k)}, \beta_5^{(k)}) \tag{57}$$

The modeling capabilities of polynomial functions are well known, e.g., Hill (1950), Gotoh (1977), and Soare et al. (2008). However, as mentioned earlier, the problem with polynomial formulations is that without additional constraints upon the identification process it is very difficult, if not impossible for $n \ge 6$, to obtain convex functions, Soare et al. (2008). The question is then whether the range of the convex parametrization introduced here is wide enough to retain as much as possible from the modeling power of polynomial functions. Not every convex parametrization is optimal. For example, in Plunkett et al. (2008) Eq. (5) was employed with a homogeneity degree of n=20 to model the aluminum alloy AA2090-T3 characterized in Barlat et al. (2005) by directional and biaxial data. On the other hand, the same modeling performance was achieved in Barlat et al. (2005) with a homogeneity degree of n=8. As illustration of the modeling capabilities of formula (45), we show here the modeling of the same alloy with sixth and eight order polynomials. Further illustrations are presented in the supplementary material attached to the electronic version of the paper.

The P_6 and P_8 modelings of AA2090-T3 aluminum alloy are presented in Fig. 5. The directional data set contains J=7 data points, while $\overline{\sigma}_b = 1.035$, r_b=0.67. Four image stresses were used for both P_6 and P_8. For P_6 the following three in-plane isotropic generators (25) were used (they were identified to give a first best fit, after which the data fit could be further improved with five more iterations):

$$\begin{aligned} &\overline{\sigma}_0 = 1.0, \quad \overline{\sigma}_b = 1.035, \quad R = 0.212, \quad P = 0.9325 \quad (\text{for } \Sigma^{(1)}) \\ &\overline{\sigma}_0 = 1.0, \quad \overline{\sigma}_b = 1.035, \quad R = 1.2, \quad P = 0.9065 \quad (\text{for } \Sigma^{(2)}) \\ &\overline{\sigma}_0 = 1.0, \quad \overline{\sigma}_b = 1.035, \quad R = 1.55, \quad P = 0.892 \quad (\text{for } \Sigma^{(3)}, \Sigma^{(4)}) \end{aligned} \tag{58}$$

The set of parameters (R, P_6) for which IP_6 is convex in the present case is shown in Fig. 6 (actually only the region of interest here). This set is the 2D slice

$$\begin{cases} \overline{\sigma}_0 = 1 \\ \overline{\sigma}_b = 1.035 \end{cases} \iff \begin{cases} a_1 = 1 \\ 2a_1 + 2a_2 + 2a_3 + a_4 = 1.035^{-6} \end{cases} \tag{59}$$

through the whole convexity domain of IP_6 in the 4D space (a_1, a_2, a_3, a_4). Two generators in Eq. (58), R=1.2 and 1.55, correspond to boundary points. This is typical of aluminum alloys since they feature yield surfaces with tight shapes and almost straight edges (close to zero curvature).

Two isotropic generators (36) were used for P_8 as follows:

$$\begin{aligned} &\overline{\sigma}_0 = 1.0 = \overline{\sigma}_b, \quad R = 0.2, \quad P_1 = 0.955, \quad P_2 = 1.4 \quad (\text{for } \Sigma^{(1)}, \Sigma^{(2)}) \\ &\overline{\sigma}_0 = 1.0 = \overline{\sigma}_b, \quad R = 0.2, \quad P_1 = 0.955, \quad P_2 = 1.55 \quad (\text{for } \Sigma^{(3)}, \Sigma^{(4)}) \end{aligned} \tag{60}$$

For P_1=0.955, the maximal interval for P_2 is [1.285, 1.581]. The whole convexity domain in this case is featured in Fig. 7, together with the position of the two generators above and, for comparison, two other vertices of the convexity domain, (0.5267,9.791) and (0.669,41.4). Polynomial coefficients and image stresses parameters for AA2090-T3 and two other examples are tabulated in the electronic Supplement of the paper.

5. Further considerations about the 3D case

We sketch in this concluding section an extension of the present theory to general 3D stress states. Having already a plane stress theory at hand, it is natural to attempt to make full use of its modeling capabilities and define the following

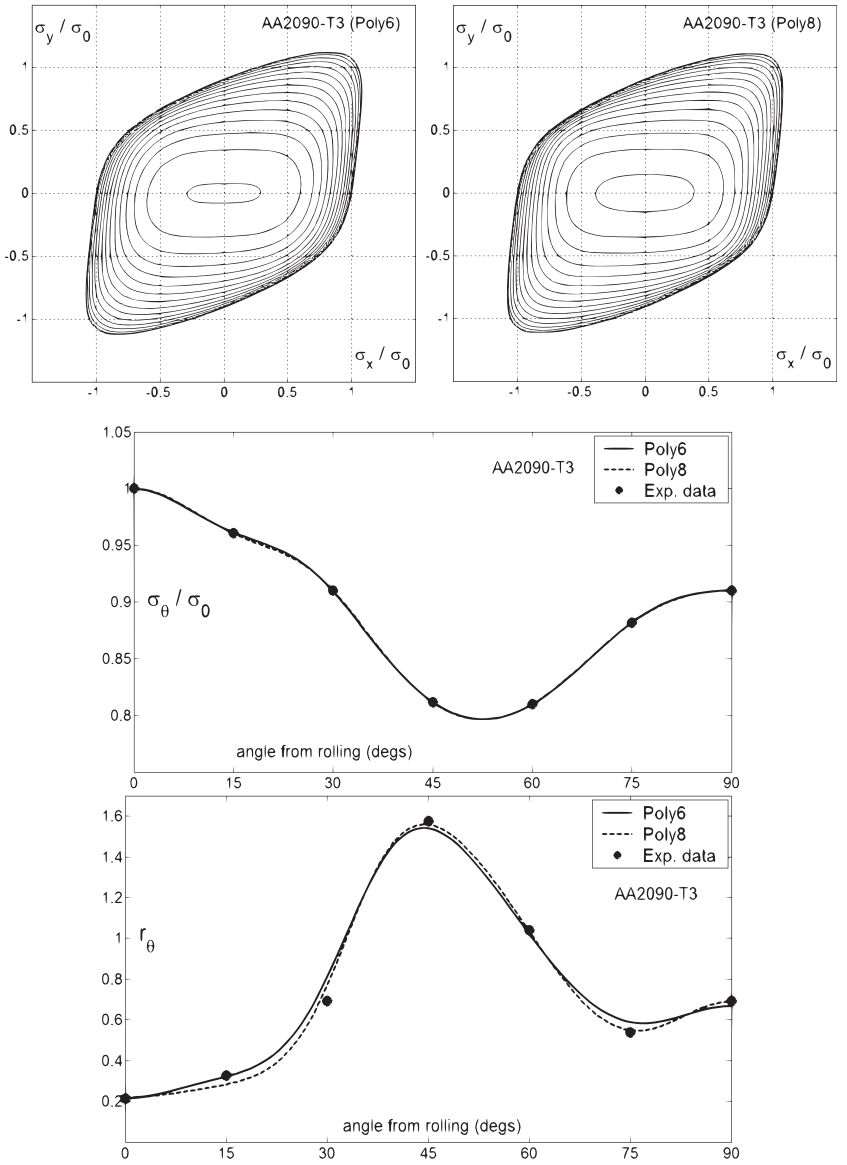

Fig. 5. Poly6 and Poly8 modeling of AA2090-T3: $\sigma_{xy} = \text{const.}$ level curves and directional properties.

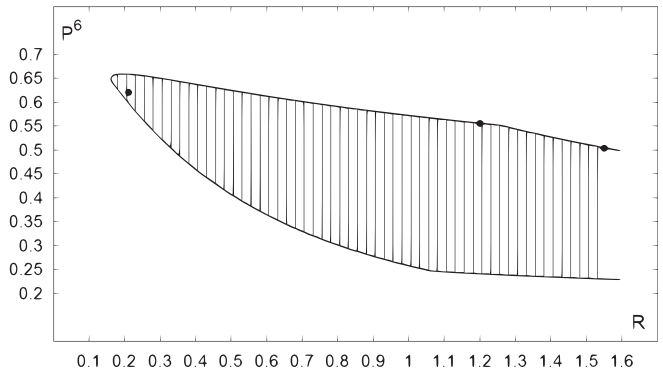

Fig. 6. The convexity domain for IP_6 when $\overline{\sigma}_0 = 1.0$, $\overline{\sigma}_b = 1.035$, $0.161 \le R \le 1.6$, and the three generators for AA2090-T3 (full circles).

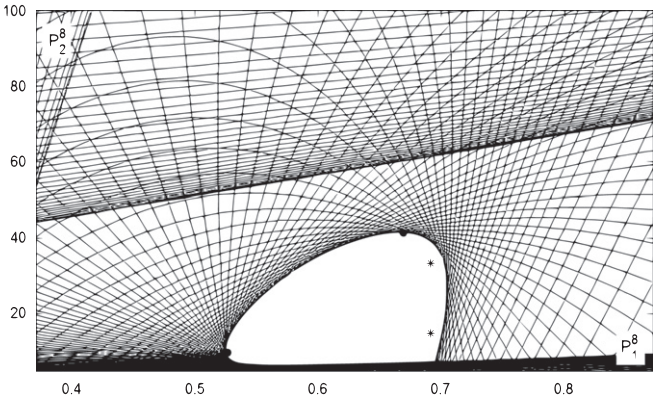

Fig. 7. Convexity set for IP_8 when $\overline{\sigma}_0=\overline{\sigma}_b=1$ and R=0.2. Also shown (stars) are the two pairs of shapes parameters corresponding to the generators used for modeling AA2090-T3, and two vertices of the convexity set (full circles).

pressure independent extension:

$$f^n(\sigma_1,\sigma_2,\sigma_3)=g_n(\sigma_1-\sigma_3,\sigma_2-\sigma_3) \tag{61}$$

of the n-th order homogeneous polynomial plane stress in-plane isotropic criterion $g_n(\sigma_1,\sigma_2)$. However, in general, the above function is no longer a polynomial since in this case the principal value σ_3 is not a linear combination of stress components and σ_1 and σ_2 are not conjugated. Polynomial forms are recovered if the following symmetric formula is employed:

$$f^n(\sigma_1,\sigma_2,\sigma_3)=g_n(\sigma_1-\sigma_3,\sigma_2-\sigma_3)+g_n(\sigma_1-\sigma_2,\sigma_3-\sigma_2)+g_n(\sigma_2-\sigma_1,\sigma_3-\sigma_1) \tag{62}$$

This is equivalent with employing formula (61) with an *isotropic* plane stress function g. The convexity of f then follows from the following two Lemmas that parallel those in Section 3.

Lemma 1b. *An isotropic pressure independent function expressed as $f(\sigma_1,\sigma_2,\sigma_3)$ in the space of principal stresses, is uniquely determined by its restriction to one of the principal planes. More precisely, if, say, $g(\sigma_1,\sigma_2)$ is the restriction of f to the plane (σ_1,σ_2), then*

$$f(\sigma)=g(\sigma_1-\sigma_3,\sigma_2-\sigma_3) \tag{63}$$

Proof. If $g(\sigma_1,\sigma_2):=f(\sigma_1,\sigma_2,0)$, then $g(\sigma_1-\sigma_3,\sigma_2-\sigma_3)=f(\sigma_1-\sigma_3,\sigma_2-\sigma_3,0)=f(\sigma_1,\sigma_2,\sigma_3)$, the last equality following from pressure independence. □

Lemma 2b. *An isotropic pressure independent function $f(\sigma)$ is convex if and only if one of its biaxial curves is convex.*

Proof. Let $f_{123}=f_{123}(\sigma_1,\sigma_2,\sigma_3)$ denote the expression of the function f in principal stresses, and $f_{xyz}=f_{xyz}(\sigma_x,\sigma_y,\sigma_z,\sigma_{xy},\sigma_{xz},\sigma_{yz})$ denote its expression in stress space (referred to a Cartesian coordinate system). Suppose the biaxial restriction $g_{xy}(\sigma_x,\sigma_y):=f(\sigma_x,\sigma_y,0,0,0,0)$ is convex and define $g_{12}(\sigma_1,\sigma_2):=f_{123}(\sigma_1,\sigma_2,0)$. Then $g_{12}(\sigma_1,\sigma_2)=g_{xy}(\sigma_1,\sigma_2)$. Hence g_{12} is convex. From Lemma 1b it follows that f_{123} is convex (since it is obtained from g_{12} by a linear transformation). Since f is isotropic, f_{123} is also symmetric. With Davis' theorem it follows that f_{xyz} is convex. □

For example, the most general isotropic and pressure independent 3D sixth order polynomial can be obtained from the plane stress isotropic sixth order polynomial, Eq. (25) with $\overline{\sigma}=\overline{\sigma}_b=R=1$:

$$IP_6^{(3D)}(\sigma)=IP_6(\sigma_1-\sigma_3,\sigma_2-\sigma_3)$$

$$a_1=1,\quad a_2=-3,\quad a_3=16P^6-3/4,\quad a_4=-(32P^6-13/2) \tag{64}$$

The parameter $P\in[0.810,0.926]$ has the same shape control properties as for plane stress conditions. In particular, for P^6=27/64, 33/64, or 243/704, one recovers the von Mises function, the HH and KB functions, respectively. Noteworthy, the J_2J_3 criterion proposed by Drucker (1949), $\overline{\sigma}^6=J_2^3-cJ_3^2$, with J_2 and J_3 the two nonzero invariants of the stress deviator, is also a one-parameter sixth order homogeneous polynomial (a particular case of the above formula). However, Drucker's approach is limited to very particular combinations of powers of the J_2 and J_3 invariants, since the next polynomial function in this approach would have a homogeneity degree of 12 (!). Similarly, the most general eight order isotropic pressure independent polynomial has two parameters and reads

$$IP_8^{(3D)}(\sigma)=IP_8(\sigma_1-\sigma_3,\sigma_2-\sigma_3)$$

$$a_1=1,\quad a_2=-4,\quad a_3=\frac{64P_1^8}{9}+\frac{P_2^8}{18}+\frac{13}{4},\quad a_4=\frac{17-P_2^8}{4},\quad a_5=\frac{7P_2^8}{18}-\frac{128P_1^8}{9}-8 \tag{65}$$

with IP_8 defined by Eq. (36), and the shape parameters P_1 and P_2 restricted to the convexity domain described in Section 3.3. Also, the 3D von Mises, HH and KB (when $n=8$) functions are obtained for the particular combinations of P_1 and P_2 described there.

Next, one could follow the path used for the plane stress case and use the above functions as generators for further anisotropic extensions by the linear transformation approach. However, part of the flexibility of the plane stress generators is lost since the average R-value of the generator can no longer be optimized. An expansion in terms of monomials $s_1^i s_2^j s_3^j$, $i+j+k=2k$, of Eq. (64) or (65), similar to the ones used for plane stress, will reveal that all basis monomials are required to form the above two isotropic functions (and, in particular, it can be used to show that they are also polynomials of the components σ_{ij} of the stress tensor). An alternative 3D formulation that reduces coupling and incorporates the general plane stress formulation of Section 4 is as follows:

$$f^n(\sigma)=g_n(\Sigma_1,\Sigma_2)+g_n(\Sigma_2,\Sigma_3)+g_n(\Sigma_3,\Sigma_1) \tag{66}$$

with Σ the image stress (4) and Σ_i its eigenvalues. Recall that Σ is pressure independent, i.e., $\Sigma(\sigma+pI)=\Sigma(\sigma)$, for any $p\in\mathbb{R}$, and hence f is pressure independent. Eq. (66) can be qualified as an HH-extension. For example, when $n=6$ the HH isotropic criterion (2) is obtained if g_6 is given by Eq. (25) with $a_1=1/2$, $a_2=-3$ and $P_6=33/64$. More generally, Eq. (66) is a polynomial of the stress components. To see this, recall that the function g_n is a linear combination of terms of the form $(\sigma_1^{n-2p}+\sigma_2^{n-2p})\sigma_1^p\sigma_2^p$, for $p=0,\ldots,n/2$, and hence

$$\begin{aligned}&\sum_{p=0}^{n/2} a_{p+1}[(\Sigma_1^{n-2p}+\Sigma_2^{n-2p})\Sigma_1^p\Sigma_2^p+(\Sigma_2^{n-2p}+\Sigma_3^{n-2p})\Sigma_2^p\Sigma_3^p+(\Sigma_3^{n-2p}+\Sigma_1^{n-2p})\Sigma_3^p\Sigma_1^p]\\ &\quad=\sum_{p=0}^{n/2} a_{p+1}[\Sigma_1^{n-p}(\Sigma_2^p+\Sigma_3^p)+\Sigma_2^{n-p}(\Sigma_1^p+\Sigma_3^p)+\Sigma_3^{n-p}(\Sigma_1^p+\Sigma_2^p)]\\ &\quad=\sum_{p=0}^{n/2} a_{p+1}[Q_{n-p}(\Sigma)Q_p(\Sigma)-Q_n(\Sigma)]=\sum_{p=0}^{n/2} b_{p+1}Q_{n-p}(\Sigma)Q_p(\Sigma)\end{aligned} \tag{67}$$

where each sum of powers $Q_i(\Sigma)=\Sigma_1^i+\Sigma_2^i+\Sigma_3^i$ is a homogeneous polynomial of the i-th degree in the stress components, Section 2, and in the last equality above the coefficients were redefined as follows: $b_1=(2a_1-a_2-\cdots)/3$ and $b_p=a_p$ for $p\geq 2$. To complete the theory of Eq. (66), if the function $\mathbb{R}^2\ni(x,y)\longrightarrow g_n^{1/n}(x,y)$ is convex, then by Minkowski's inequality the function ϕ defined by $\mathbb{R}^3\ni(x,y,z)\longrightarrow\phi^n(x,y,z):=g_n(x,y)+g_n(y,z)+g_n(z,x)$ is also convex and since ϕ is also symmetric, by Davis' theorem (Section 2) the function (66) is convex, as a function of the stress tensor σ.

Finally, to add more parameters for increased modeling power, one can follow the approach tested in Section 4 and write

$$f^n(\sigma)=\frac{1}{K}\sum_{k=1}^{K} f_{(k)}^n(\sigma) \tag{68}$$

where each $f_{(k)}$ corresponds to an image stress $\Sigma^{(k)}$. For relatively small data sets, directional and biaxial properties, two image stresses, and hence two functions in the sum above, are in general sufficient. The identification procedure of those parameters entering the description of a plane stress state follows the same algorithm as described in Section 4. For the rest of the parameters additional data points (from experiments or polycrystal calculations) must be supplied. As an application of formulas (67) and (68) we recover the Yl2004 parametrization, Eq. (10). Its polynomial reformulation (15) can be decomposed as

$$2f^n(\sigma)=\sum_{p=0}^{n/2} b_{p+1}^{(1)}Q_{n-p}(\Sigma^{(1)})Q_p(\Sigma^{(1)})+\sum_{p=0}^{n/2} b_{p+1}^{(2)}Q_{n-p}(\Sigma^{(2)})Q_p(\Sigma^{(2)}) \tag{69}$$

with $b_{p+1}^{(1)}=2(-1)^pC_n^pQ_p(\Sigma^{(2)})/Q_p(\Sigma^{(1)})$, $b_{p+1}^{(2)}=2(-1)^pC_n^pQ_p(\Sigma^{(1)})/Q_p(\Sigma^{(2)})$, for $p=n/2$ the corresponding coefficients being halved. The advantage brought by the Yld2004 parametrization is now apparent: it eliminates the preliminary step of choosing the shape parameters for the g-generators. However, with this simplification the range of the b parameters is now a strict subset of the whole convexity domain. The implementation details of Yld2004 in the polynomial form are further discussed in Appendix B.

Acknowledgement

S.S. was partly supported by the National Council for Research and Innovation of Romania (through Grant 4/30.04.2008 RP4).

Appendix A. Coefficients of the convexity quadratics for IP_6 and IP_8

The coefficients c_{ij} of the IP_6 quadratic (32) are

$$c_{11}=\tfrac{45}{32}[3-4\cos(4\omega)+\cos(8\omega)],\quad c_{12}=\tfrac{15}{4}[3\sin(2\omega)-\sin(6\omega)]$$

$$c_{13}=\tfrac{3}{16}[65+4\cos(4\omega)-5\cos(8\omega)],\quad c_{14}=\tfrac{9}{8}[7\sin(2\omega)+3\sin(6\omega)]$$

$$c_{22}=\tfrac{5}{32}[-7+3\cos(8\omega)-28\cos(4\omega)],\quad c_{23}=\tfrac{1}{4}[5\sin(2\omega)-7\sin(6\omega)]$$

$$c_{24}=\tfrac{3}{32}[5-\cos(8\omega)-4\cos(4\omega)],\quad c_{33}=\tfrac{1}{32}[-17+5\cos(8\omega)+12\cos(4\omega)]$$

$$c_{34}=\tfrac{3}{8}[-3\sin(2\omega)+\sin(6\omega)],\quad c_{44}=\tfrac{9}{128}[-3-\cos(8\omega)+4\cos(4\omega)]$$

The coefficients c_{ij} of the IP_8 quadratic (40) are

$$c_{11}=\tfrac{1}{32}[42\cos(8\omega)-105\cos(4\omega)-7\cos(12\omega)+70]$$

$$c_{12}=\tfrac{1}{32}[210\sin(2\omega)-105\sin(6\omega)+21\sin(10\omega)]$$

$$c_{13}=\tfrac{1}{4}[15\cos(4\omega)+6\cos(8\omega)+\cos(12\omega)+42]$$

$$c_{14}=\tfrac{1}{32}[378\sin(2\omega)+155\sin(6\omega)-15\sin(10\omega)]$$

$$c_{15}=\tfrac{1}{32}[126-45\cos(4\omega)-3\cos(12\omega)-78\cos(8\omega)]$$

$$c_{22}=\tfrac{1}{512}[126\cos(8\omega)-2625\cos(4\omega)-63\cos(12\omega)-1022]$$

$$c_{23}=\tfrac{1}{16}[24\sin(2\omega)-45\sin(6\omega)+3\sin(10\omega)]$$

$$c_{24}=\tfrac{1}{256}[6\cos(8\omega)-405\cos(4\omega)+21\cos(12\omega)+378]$$

$$c_{25}=\tfrac{1}{64}[90\sin(2\omega)-5\sin(6\omega)-15\sin(10\omega)]$$

$$c_{33}=\tfrac{1}{32}[18\cos(8\omega)-15\cos(4\omega)-\cos(12\omega)-2]$$

$$c_{34}=\tfrac{1}{16}[3\sin(10\omega)-5\sin(6\omega)]$$

$$c_{35}=0$$

$$c_{44}=\tfrac{1}{512}[135\cos(4\omega)-18\cos(8\omega)-7\cos(12\omega)-110]$$

$$c_{45}=\tfrac{1}{64}[15\sin(6\omega)-30\sin(2\omega)-3\sin(10\omega)]$$

$$c_{55}=\tfrac{1}{128}[15\cos(4\omega)-6\cos(8\omega)+\cos(12\omega)-10]$$

Appendix B. Yld2004 FE and parameters identification implementation details

As shown in Section 2, the Yld2004 yield function admits the following polynomial form:

$$f^n(\sigma)=\sum_{p=0}^{n}(-1)^p C_n^p Q_{n-p}(\Sigma^{(1)})Q_p(\Sigma^{(2)}) \tag{B.1}$$

where $Q_p \coloneqq S_1^p+S_2^p+S_3^p$. An FE implementation requires computation of the value $f(\sigma)$, gradient $Df(\sigma)$, and hessian $Hf(\sigma)$ (for implicit codes). All can be computed explicitly and fast, even for high homogeneity degrees, by using the recurrence formula

$$Q_p=I_1Q_{p-1}+I_2Q_{p-2}+I_3Q_{p-3},\quad p\geq 3 \tag{B.2}$$

with

$$Q_0\coloneqq 3,\quad Q_1\coloneqq S_1+S_2+S_3=I_1,\quad Q_2\coloneqq S_1^2+S_2^2+S_3^2=\Sigma\cdot\Sigma=I_1^2+2I_2 \tag{B.3}$$

Starting the loop requires computing first the invariants

$$I_1\coloneqq \mathrm{tr}(\Sigma),\quad I_2\coloneqq(\Sigma\cdot\Sigma-I_1^2)/2,\quad I_3\coloneqq\det(\Sigma) \tag{B.4}$$

and the derivatives:

$$\frac{\partial I_1}{\partial \Sigma_{ij}} = \delta_{ij}, \quad \frac{\partial^2 I_1}{\partial \Sigma_{ij}\partial \Sigma_{pq}} = 0, \quad \frac{\partial I_2}{\partial \Sigma_{ij}} = \Sigma_{ij} - I_1\delta_{ij}, \quad \frac{\partial^2 I_2}{\partial \Sigma_{ij}\partial \Sigma_{pq}} = \delta_{ip}\delta_{jq} - \delta_{pq}\delta_{ij} \tag{B.5}$$

$$\frac{\partial I_3}{\partial \Sigma_{ij}} = (-1)^{i+j}\Sigma_{ij}\det(M_{ij}) \tag{B.6}$$

$$\frac{\partial^2 I_3}{\partial \Sigma_{ij}\partial \Sigma_{pq}} = (-1)^{i+j}[\delta_{ip}\delta_{jq}\det(M_{ij}) + \Sigma_{ij}(-1)^{p+q}\Sigma_{pq}\det(N_{pq})(1-\delta_{ip})(1-\delta_{jq})] \tag{B.7}$$

$$\Sigma_{ij} \coloneqq T_{ijpq}\sigma_{pq} \Rightarrow \frac{\partial \Sigma_{ij}}{\partial \sigma_{pq}} = T_{ijpq} \tag{B.8}$$

where, to ease the notation, we have adopted an index notation for stress components, and where M_{ij} is the matrix obtained from Σ by eliminating line i and column j, while N_{pq} is the matrix obtained from M_{ij} by eliminating line p and column q.

The parameter identification procedure requires computation of the function value and its gradient, and derivatives with respect to the material parameters. In this case, storing the variables in vector/matrix form so that we can write

$$[\Sigma] = [\beta][\sigma] \Longleftrightarrow \Sigma_i = \beta_{ij}\sigma_j \tag{B.9}$$

reduces the last task to

$$\partial \Sigma_i / \partial \sigma_j = \beta_{ij} \tag{B.10}$$

Appendix C. Supplementary data

Supplementary data associated with this article can be found in the online version at doi:10.1016/j.jmps.2010.08.005.

References

Barlat, F., 1987. Crystallographic texture, anisotropic yield surfaces and forming limit diagrams. Mater. Sci. Eng. 91, 55–72.
Barlat, F., Lege, D.J., Brem, J.C., 1991. A six-component yield function for anisotropic materials. Int. J. Plast. 7, 693–712.
Barlat, F., Aretz, H., Yoon, J.W., Karabin, M.E., Brem, J.C., Dick, R.E., 2005. Linear transformation based anisotropic yield function. Int. J. Plast. 21, 1009–1039.
Barlat, F., Yoon, J.W., Cazacu, O., 2007. On linear transformations of stress tensors for the description of plastic anisotropy. Int. J. Plast. 23, 876–896.
Bassani, J.L., Hutchinson, J.W., Neale, K.W., 1979. On the prediction of necking in anisotropic sheets. In: Lippmann, H. (Ed.), Metal Forming Plasticity. Springer-Verlag, Berlin.
Bishop, J.W.F., Hill, R., 1951a. A theory of the plastic distortion of a polycrystalline aggregate under combined stresses. Philos. Mag. 42, 414–427.
Bishop, J.W.F., Hill, R., 1951b. A theoretical derivation of the plastic properties of polycrystalline face-centered metals. Philos. Mag. 42, 1298–1307.
Boehler, J.P., 1987. Application of Tensors Functions in Solids Mechanics, CISM Courses and Lectures, vol. 292. Springer, Berlin.
Bron, F., Besson, J., 2004. A yield function for anisotropic materials. Application to aluminum alloys. Int. J. Plast. 20, 937–963.
Davis, C., 1957. All convex invariant functions of hermitian matrices. Arch. Math. 8, 276–278.
Drucker, D.C., 1949. Relation of experiments to mathematical theories of plasticity. J. Appl. Mech. 16, 349–357.
Flanders, H., 1968. A proof of Minkowski's inequality for convex curves. Am. Math. Mon. 75, 581–593.
Gotoh, M., 1977. A theory of plastic anisotropy based on a yield function of fourth order (plane stress)—part I and II. Int. J. Mech. Sci. 19, 505–520.
Hershey, A.V., 1954. The plasticity of an isotropic aggregate of anisotropic face centered cubic crystals. J. Appl. Mech. 21, 241–249.
Hill, R., 1950. The Mathematical Theory of Plasticity. Clarendon Press, Oxford.
Hosford, W.F., 1972. A generalized isotropic yield criterion. J. Appl. Mech. 39, 607–609.
Karafillis, A.P., Boyce, M.C., 1993. A general anisotropic yield criterion using bounds and a transformation weighting tensor. J. Mech. Phys. Solids 41, 1859–1886.
Lian, J., Barlat, F., Baudelet, B., 1989. Plastic behavior and stretchability of sheet metals. Part II: effect of yield surface shape on sheet forming limit. Int. J. Plast. 5, 131–147.
Liu, I.-S., 1982. On representations of anisotropic invariants. Int. J. Eng. Sci. 20, 1099–1109.
Plunkett, B., Cazacu, O., Barlat, F., 2008. Orthotropic yield criteria for description of anisotropy in tension and compression of sheet metals. Int. J. Plast. 24, 847–866.
Rice, J.R., 1971. Inelastic constitutive relations for solids: an internal-variable theory and its application to metal plasticity. J. Mech. Phys. Solids 19, 433–455.
Schmid, E., 1931. Beiträge zur physik und metallographie de magnesiums. Z. Electrochem. 37, 447–459.
Soare, S., Yoon, J.-W., Cazacu, O., 2008. On the use of homogeneous polynomials to develop anisotropic yield functions with applications to sheet forming. Int. J. Plast. 24, 915–944.
Soare, S., Banabic, D., 2008. About the mechanical data required to describe the anisotropy of thin sheets to correctly predict the earing of deep-drawn cups. In: Esaform 2008, Conference Proceedings.
Soare, S., 2010. Theoretical considerations upon the MK model for limit strains prediction: the plane strain case, strain-rate effects, yield surface influence and material heterogeneity. Eur. J. Mech. A/Solids, doi: 10.1016/j.euromechsol.2010.05.008.
Taylor, G.I., 1938. Plastic strains in metals. J. Inst. Metals 62, 307–324.
Wang, C.C., 1970. A new representation theorem for isotropic functions, parts I and II. Arch. Ration. Mech. Anal. 36, 166–223.
Yoon, J.-W., Barlat, F., Dick, R.E., Karabin, M.E., 2006. Prediction of six or eight ears in a drawn cup based on a new anisotropic yield function. Int. J. Plast. 22, 174–193.